# Chemical Vapor Deposition Growth of Crystalline Monolayer $MoSe_2$

Xingli Wang,[†,‡,∥] Yongji Gong,[§,∥] Gang Shi,[†] Wai Leong Chow,[‡] Kunttal Keyshar,[†] Gonglan Ye,[†] Robert Vajtai,[†] Jun Lou,[†] Zheng Liu,[‡,⊥,#] Emilie Ringe,[†,§,*] Beng Kang Tay,[‡,#,*] and Pulickel M. Ajayan[†,§,*]

[†]Department of Materials Science & NanoEngineering, Rice University, Houston, Texas 77005, United States, [‡]NOVITAS, Nanoelectronics Centre of Excellence, School of Electrical and Electronic Engineering, Nanyang Technological University, 639798 Singapore, [§]Department of Chemistry, Rice University, Houston, Texas 77005, United States, [⊥]School of Materials Science and Engineering, Nanyang Technological University, 639798 Singapore, and [#]CNRS-International-NTU-Thales Research Alliance (CINTRA), Nanyang Technological University, 639798 Singapore. [∥]X.W. and Y.G. contributed equally to this work.

**ABSTRACT**

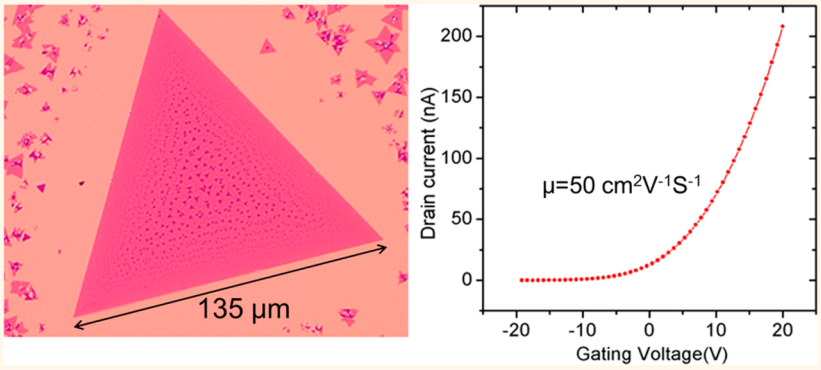


Recently, two-dimensional layers of transition metal dichalcogenides, such as $MoS_2$, $WS_2$, $MoSe_2$, and $WSe_2$, have attracted much attention for their potential applications in electronic and optoelectronic devices. The selenide analogues of $MoS_2$ and $WS_2$ have smaller band gaps and higher electron mobilities, making them more appropriate for practical devices. However, reports on scalable growth of high quality transition metal diselenide layers and studies of their properties have been limited. Here, we demonstrate the chemical vapor deposition (CVD) growth of uniform $MoSe_2$ monolayers under ambient pressure, resulting in large single crystalline islands. The photoluminescence intensity and peak position indicates a direct band gap of 1.5 eV for the $MoSe_2$ monolayers. A back-gated field effect transistor based on $MoSe_2$ monolayer shows n-type channel behavior with average mobility of 50 $cm^2\ V^{-1}\ s^{-1}$, a value much higher than the 4—20 $cm^2\ V^{-1}\ s^{-1}$ reported for vapor phase grown $MoS_2$.

**KEYWORDS:** transition metal dichalcogenides · molybdenum diselenide · transistors · two-dimensional materials · chemical vapor deposition · monolayer

Monolayer transition metal dichalcogenides (TMDs) such as $MoS_2$ have recently attracted tremendous interest due to their narrow band gap (ranging from 1.1 for $MoTe_2$ to 2.0 eV for $WS_2$),[1−3] indirect to direct band gap transition, efficient hydrogen evolution when used as catalysts,[1−6] *etc.*, enabling a wide range of applications from electronics and optoelectronics to energy conversion.[7−13] Among the more than 40 types of compounds in the TMD family, $MoS_2$ is arguably the most extensively studied due to its promising semiconducting properties. Studies indicate that the less well-studied selenides may however be superior to sulfides in many aspects owing to a narrower band gap (1.5 eV in $MoSe_2$ *vs* 1.9 eV in $MoS_2$), a 10-fold narrower line width, and tunable excitonic charging effects.[14,15] While progress in synthetic methodologies allows for monolayer and single-crystal growth of $MoS_2$ with lateral dimensions reaching hundreds of micrometers,[16,17] there remain significant challenges related to controlled, reproducible, and large area growth of the selenides.

Monolayer molybdenum diselenide ($MoSe_2$) is in fact a "three-layer" structure consisting of top and bottom Se layers sandwiching Mo layers.[2] In multilayer arrangements, layers are stacked together with weak van der Waals

* Address correspondence to emilie.ringe@rice.edu, ebktay@ntu.edu.sg, ajayan@rice.edu.

Received for review February 27, 2014 and accepted March 28, 2014.

**Published online March 29, 2014**
**10.1021/nn501175k**

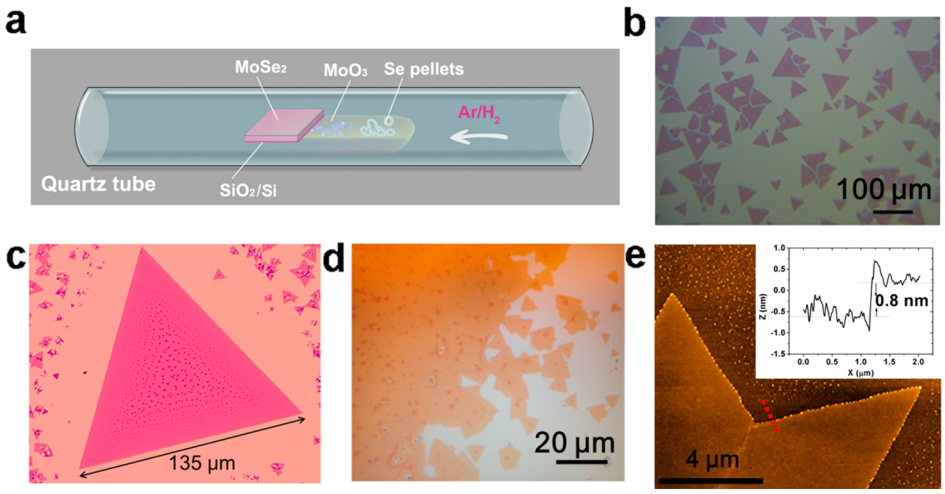


**Figure 1. $MoSe_2$ monolayer synthesis and morphology. (a) Schematic of the controlled synthesis of monolayer $MoSe_2$ *via* CVD. Se pellets and $MoO_3$ powder are positioned in same ceramic boat at the center of the tube furnace. (b–d) Typical optical images of monolayer triangles and continuous film. Small bilayer domains with darker color can be observed in (c) and (d). (e) AFM height topography of monolayer $MoSe_2$, and the height profile (inset) showing a thickness of ~0.8 nm, as measured along the red dotted line.**

interactions between Se atoms; in this "bulk" form, $MoSe_2$ has been used as a host for intercalation,[18] lubricants,[19] catalysts,[20] and electrodes.[21] Akin to $MoS_2$ and $WSe_2$,[1,5,22] the band structure of $MoSe_2$ varies with the number of layers. Decreasing thickness changes the band structure of $MoSe_2$ from indirect (as in a bulk crystal) to direct (as in a monolayer); meanwhile, the band gap increases from 1.1 to 1.5 eV.[15] Such tunable properties of $MoSe_2$ render it an ideal material for various electrical and optical applications. Recently, back-gated field effect transistors were fabricated on ultrathin $MoSe_2$ films,[23] achieving an on/off ratio as high as $10^6$ and an intrinsic mobility up to ~50 $cm^2\ V^{-1}\ s^{-1}$ at room temperature, which was shown to increase nearly 4-fold at 78 K. Given such properties, monolayer to few-layers $MoSe_2$ appears to be a tremendous candidate for applications in electrical and optical devices.

However, synthesis of good quality, large-scale $MoSe_2$ remains a challenge, with very few methods reported.[25−29] Several chemical approaches produce $MoSe_2$ nanocrystals, such as the sonochemical reaction between $Mo(CO)_6$ and Se at 0 °C[24] and the solvothermal conversion of $MoO_3$ to $MoSe_2$.[25] Much like graphene and other 2d materials,[26] exfoliation of bulk $MoSe_2$, with[27] or without[23] sonication, can be used to produce monolayers for fundamental studies. Large size $MoSe_2$ single crystals were recently synthesized by chemical vapor transport with $TeCl_4$ by Bougouma *et al.*[28] Nevertheless, these syntheses are restricted to either "bulk" material (nanocrystals) or few layers with limited size and quality.

Beyond exfoliation, chemical vapor deposition (CVD) has been demonstrated to be a successful approach to synthesize various 2D materials, such as graphene,[29−31] h-BN,[32,33] $MoS_2$,[16,17,34] $WS_2$,[35,36] and $WSe_2$.[37] Here, we extend this approach and report the synthesis of monolayer $MoSe_2$ by a CVD method under atmospheric pressure. With a direct optical band gap of 1.48 eV, as seen in photoluminescence (PL, peak at 840 nm), this 2D material appears ideally suited for applications in optoelectronics. We fabricated field effect transistors (FET) on the CVD grown samples, which show that $MoSe_2$ monolayers work as an n-type channel with an average mobility of 50 $cm^2\ V^{-1}\ s^{-1}$.

## RESULTS AND DISCUSSION

$MoSe_2$, an interesting 2D optoelectronic material owing to its small, direct optical bandgap, was synthesized *via* CVD, characterized with photoluminescence spectroscopy and electron microscopy, and implemented in a field effect transistor (FET). $MoSe_2$ was grown from $MoO_3$ and selenium on a clean Si wafer with a 275 nm $SiO_2$ top layer as shown in Figure 1a. A mixture of argon and hydrogen (15% hydrogen) was used as the carrier gas and reducing atmosphere during the deposition process. Hydrogen is essential for the growth of $MoSe_2$; without it deposition does not occur, as reported in the $WSe_2$ system.[37] Growth at 750 °C for 20 min yielded a high coverage of triangular domains, as shown in Figure 1b,c. The size of the triangles ranges from several tens to more than a 100 $\mu$m. Some triangles also exhibit small domains of double layer $MoSe_2$; they appear in optical images as darker areas. Their occurrence may indicate the presence of defects in the first layer, which act as nucleation sites for the second layer growth. Similar to CVD grown $MoS_2$, $MoSe_2$ islands can merge together, forming a continuous film as shown in Figure 1d. The thickness of a grown triangle, 0.8 nm as measured by atomic force microscopy (AFM, Figure 1e), confirms that the sample is a monolayer; the domain-to-domain and film thickness homogeneity are

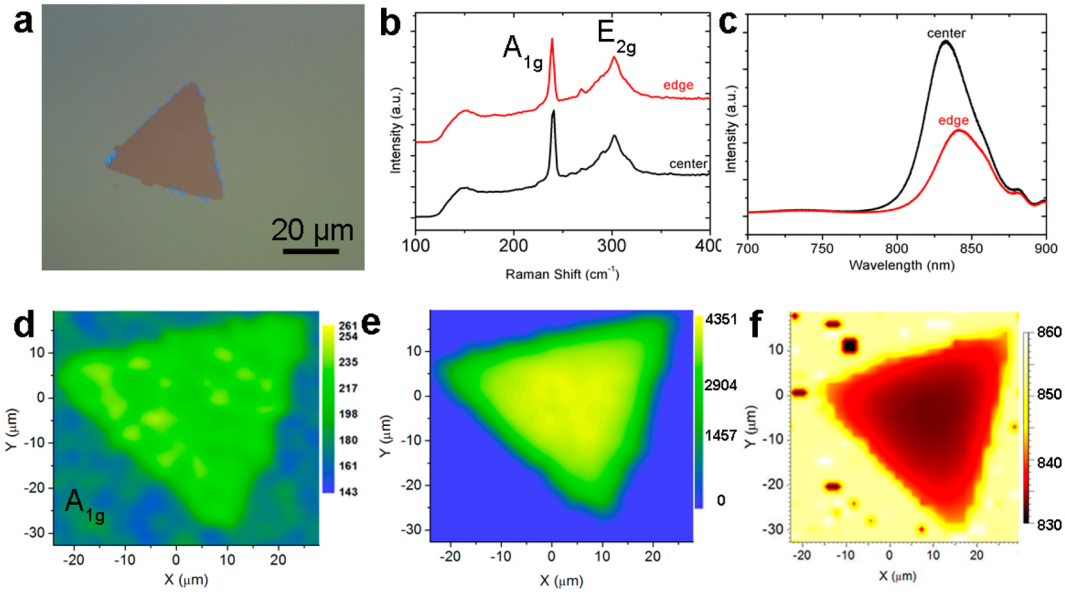


**Figure 2. Raman and PL characterization of monolayer $MoSe_2$. (a) Optical image of a small $MoSe_2$ monolayer triangle. (b) Raman spectrum at the center (black line) and edge (red line) of the triangle. (c) PL spectra at the center (black) and edge (red). (d) Raman mapping ($A_{1g}$ mode) of the triangle. (e and f) PL intensity and peak position maps.**

evidenced by the homogeneity in color present in the optical micrographs shown in Figure 1.

Raman and PL are effective methods for the characterization of crystal quality and band gap in 2D materials.[38,39] A triangle with an edge of about 40 $\mu$m (Figure 2a) was characterized with Raman and PL with a laser wavelength of 514.5 nm. Spectra were collected at the edge and center of the triangular domain, as shown in Figure 2. Two main peaks appear in the Raman spectra: a sharp one at low wavenumber (239 $cm^{-1}$) characteristic of the $A_{1g}$ mode of $MoSe_2$ (out of plane vibration) and a broad one at higher wavelength (301 $cm^{-1}$) characteristic of the $E_{2g}$ mode (in-plane vibration).[40,41] The nearly identical peak position and relative intensity in the edge and center spectra suggest a high homogeneity of the grown $MoSe_2$. The uniformity of the Raman intensity map of the 239 $cm^{-1}$ peak ($A_{1g}$ mode, Figure 2d) further confirms this observation. However, both PL spectra (Figure 2c) and PL peak intensity map (Figure 2e) show a stronger signal in the center of the triangle, with a decreased intensity at the edges. Only one high intensity peak at around 840 nm is present in both spectra, corresponding to a band gap of 1.48 eV, in excellent agreement with the reported 1.5 eV for monolayer $MoSe_2$. Under same measurement conditions, the PL spectrum of the central area of the triangle displays a peak at 830 nm, while that of the edge is redshifted to 845 nm with lower intensity. The disparity in intensity and peak energy at different positions is obvious in the PL maps. In the PL intensity map shown in Figure 2e, the center part of the triangle is clearly brighter, and the intensity decreases to about half at the edge. In the peak position map shown in Figure 2f, a red-shift from the center to the edge is observed. A related phenomenon has been reported by Peimyoo *et al.* for $WS_2$,[35] albeit in their case the edges had the highest intensity. The explanation given by Peimyoo is that the low PL intensity results from defects within the crystal, which can quench the intrinsic PL or act as nonradiative recombination sites.[35] Thus, here, we believe that the lower PL intensity at the edge is analogously caused by defects, which are more common around the edges. We also believe that such defects, in particular Se deficiencies, are responsible for the red-shift of the PL peak position and associated apparent reduction of the bandgap at the edges.[35] We observe a similar phenomenon in our PL maps of monolayer $MoS_2$.

The crystal quality of the CVD grown $MoSe_2$ was characterized at the atomic level using transmission electron microscopy (TEM) and aberration-corrected scanning TEM (STEM). A $MoSe_2$ sample with tens of micrometers domain size was transferred to a TEM grid following a poly(methyl methacrylate) (PMMA) assisted method.[16,17] The continuity of the transferred film (Figure 3a) indicated the high quality of the grown sample; folds and small particles observed on the TEM specimen were caused by the transfer process. The large domains, of the order of tens of micrometers, observed in TEM confirm the high quality produced by CVD growth. The expected hexagonal packing of single layer $MoSe_2$ is clearly observed in the atomic resolution high-angle annular dark field (HAADF) STEM images in Figure 3. In HAADF-STEM, the image intensity is directly related to atomic number, and the expected alternating brighter (2 Se) and darker (Mo) sites are clearly observed in the images and intensity profile presented in Figure 3.[42] $MoSe_2$ sample with bilayer domains were

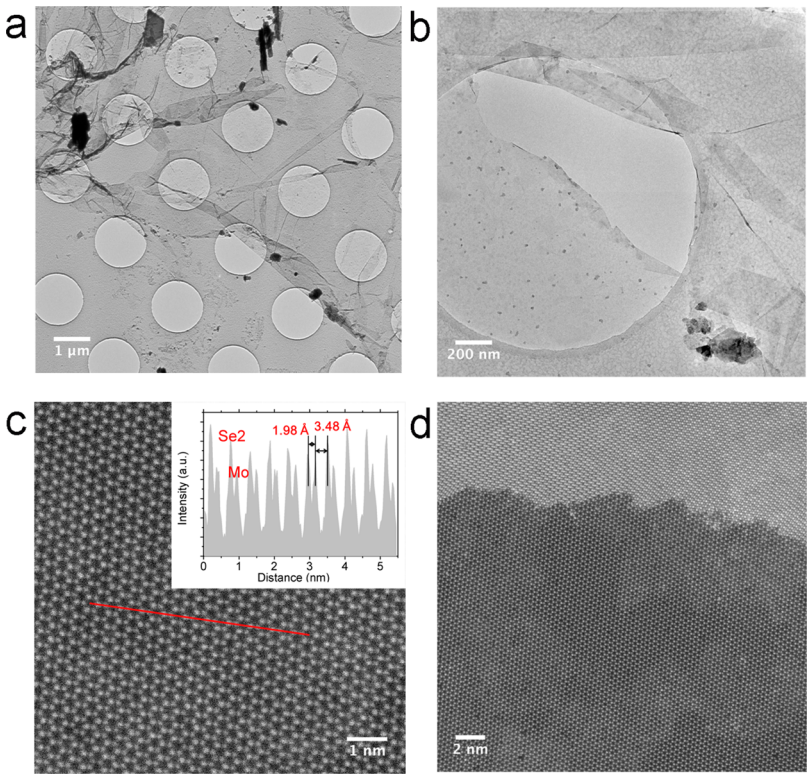


**Figure 3. Electron microscopy characterization of the sample. (a) TEM image of a monolayer $MoSe_2$ transferred to a TEM grid. The folds and black dots were produced during the transfer onto the grid. The continuousness of the film indicates the good quality of the sample. (b) TEM image of a magnified view of the resulting monolayer film. (c) STEM-HAADF image of monolayer $MoSe_2$ shows its perfect hexagonal lattice, (inset) intensity profile acquired along the red line, neighboring Mo (weak) and $Se_2$ (bright) sites are separated by 1.98 Å and the Mo−Mo distance is 5.46 Å. (d) STEM-HAADF image with interface of monolayer and double layer $MoSe_2$.**

also characterized by STEM, as shown in Figure 3d, where the bottom part is monolayer $MoSe_2$ with a perfect crystal lattice, and the brighter top part is a bilayer stacking. Additional images showing the $MoSe_2$ lattice as well as bi- and trilayer stacking can be found in the Supporting Information.

Elemental composition and bonding in the CVD grown film was examined with X-ray photoelectron spectroscopy (XPS). Four elements are present in the spectra acquired (an example is reported in Figure 4): Mo and Se from the monolayer $MoSe_2$, as well as Si and O from the $SiO_2$ substrate. The 3d spectra of Mo and Se in the $MoSe_2$ sample (Figure 4) provide information not only about stoichiometry but also about bonding. Mo $3d_{3/2}$ and $3d_{5/2}$ core levels peaks are located at ~231.5 and 228.3 eV, respectively, while the peak of Se 3d is located around 54.0 eV, in agreement with the values obtained in other $MoSe_2$ systems.[28,42] The former positions indicate the reduction of Mo from $Mo^{6+}$ to $Mo^{4+}$: peaks are significantly shifted from their hexavalent position of ~235.90 and 232.50 eV (Mo $3d_{3/2}$ and $3d_{5/2}$ core levels of $MoO_3$).[28] The peak of Se around 54.0 eV can be divided into Se $3d_{5/2}$ and Se $3d_{3/2}$ with peak positions at 53.9 and 54.7 eV, respectively.[37] Also, the 1:1.97 Mo/Se ratio obtained from high-resolution XPS suggests that the CVD grown $MoSe_2$ is reasonably

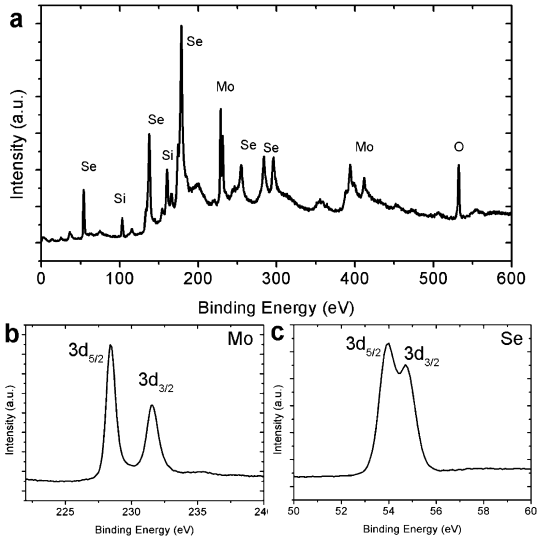


**Figure 4. XPS characterization of monolayer $MoSe_2$. (a) XPS spectrum of the sample. Four elements are present: Mo and Se (from the sample), Si and O (from the substrate). (b) XPS spectrum of Mo 3d and (c) XPS spectrum of Se 3d.**

stoichiometric. XPS indicates that there is some selenium deficiency in our $MoSe_2$ samples; such deficiencies are associated with defects and are believed to cause the PL shift and intensity decrease observed (Figure 2). The XPS elemental analysis was confirmed by electron-energy

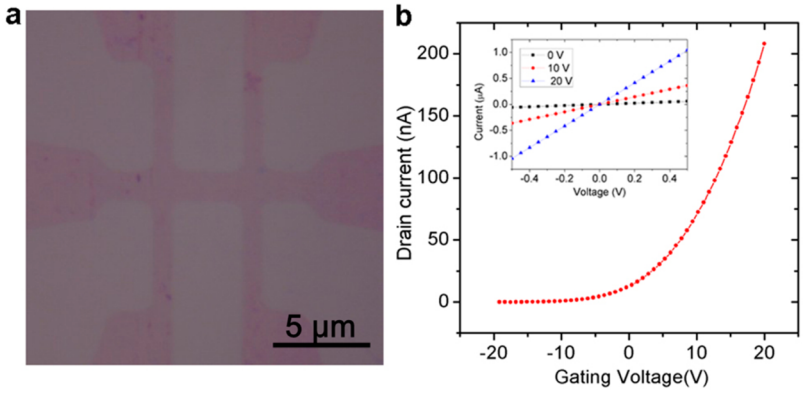


**Figure 5. Field-effect transistor (FET) device from the CVD grown $MoSe_2$ monolayer. (a) Optical image of the fabricated device. (b) Typical plot of gating voltage *vs* source/drain current (the source/drain voltage is fixed at 0.5 V). Inset: Corresponding *I*−*V* curves at different gating voltages.**

loss spectroscopy (EELS), in which both the Se and Mo edges were found (Supporting Information Figure S2).

To evaluate the electrical performance of the material, FETs were fabricated by electron-beam lithography. Figure 5a shows a typical optical micrograph of the fabricated device with a channel length and width of 10 and 2 $\mu$m, respectively. It has been discussed by a few authors that defects in TMDs can impact their electronic transport properties, specifically grain boundaries which have been demonstrated to undermine the performance of TMD transistors.[16,17] Experimentally, we are conscious of this phenomenon and have avoided the second layer when making FET devices for consistency (for example, the optical image of our FET device in Figure 5a). The typical electrical performance data of $MoSe_2$ FETs is presented in Figure 5b; all the fabricated devices displayed n-type behavior, consistent with results from mechanically exfoliated samples.[23] Field effect electron mobilities can be estimated using the equation $\mu = [dI_d/dV_{bg}] \times [L/(WC_gV_d)]$, where $L$, $W$, and $C_g$ are the channel length, width, and the gate capacitance per unit area, respectively.[9,43] Here, 0.5 V was used for the $V_d$. The *I*−*V* curves (inset in Figure 5b) confirm the Ohmic contact between the tested materials and the electrodes. From the data acquired for the $MoSe_2$ FET shown in Figure 5b, the on/off current ratio was found to exceed $10^6$, while the electron mobilities are within 20−80 $cm^2\ V^{-1}\ s^{-1}$, with an average mobility of 50 $cm^2\ V^{-1}\ s^{-1}$. The similarity of this result to that for exfoliated $MoSe_2$ monolayer[23] is a strong evidence of the high quality of the CVD grown sample. It is worth emphasizing that the electron mobility of the resulting $MoSe_2$ is much higher than that of CVD $MoS_2$ when measured by the same back-gated configuration (3−20 $cm^2\ V^{-1}\ s^{-1}$).[16,17]

## CONCLUSION

In conclusion, we have demonstrated the CVD growth of monolayer $MoSe_2$ single crystalline islands and films. The resulting $MoSe_2$ is large in area, uniform, highly crystalline and has a stoichiometry very near 1:2. The direct band gap of 1.48 eV indicated by PL indicates its possible application as a semiconductor; its back-gated FET performance shows $MoSe_2$ as a candidate for 2D semiconductor device application with an average mobility of 50 $cm^2\ V^{-1}\ s^{-1}$ and on/off ratio of $10^6$.

## METHODS

**Growth of $MoSe_2$.** To synthesize monolayer $MoSe_2$, CVD method has been developed. Selenium pellets (99.9%, Sigma Aldrich) and molybdenum oxide ($MoO_3$) (99%, Sigma Aldrich) powder, as Se and Mo precursor, respectively, were placed into the same alumina boat. A clean Si wafer with a 275 nm $SiO_2$ top layer was placed face down in the boat. The boat with precursor and substrate was in a fused quartz tube and located at the center of the reactor, *i.e.*, the hot zone. The furnace temperature was raised up to 750 °C with a heating ramp of 50 °C/min and, after that, was held at 750 °C for 20 min, yielding $MoSe_2$ triangle domains or films. After growth, the furnace was left to cool unassisted. During all the process, 50 sccm mixture of argon and hydrogen (15% hydrogen) was used as the carrier gas and reducing atmosphere during the deposition process. The growth was carried on under atmospheric pressure.

**TEM Sample Preparation and Characterization.** The TEM sample is prepared by a PMMA assisted method.[16,17] First, a PMMA thin film was spin-coated on the top of the $MoSe_2/SiO_2/Si$ substrate. After that, the $SiO_2$ layer was etched by 2 M KOH solution and the PMMA/$MoSe_2$ layer would lift off. The PMMA/$MoSe_2$ was then transferred onto the TEM grid (perforated carbon film with an orthogonal array of 1.2 $\mu$m diameter holes and 1.3 $\mu$m separation, mounted on a 200 mesh Au grid, Ted Pella) and air-dried; PMMA was subsequently washed off with acetone and 2-propanol.

The TEM images in Figure 3a,b were recorded at 200 kV on a JEOL 2100F. The HAADF-STEM images in Figure 3c,d were recorded on an aberration-corrected JEOL ARM CFEG operated at 80 kV.

**FET Device Fabrication.** Contacts consisting of 3 nm titanium and 35 nm gold were fabricated by e-beam evaporation. The rate of deposition of titanium was maintained at 0.01 nm/s. After the deposition, the devices were baked for 2 h at 120 °C under vacuum.

*Conflict of Interest:* The authors declare no competing financial interest.

*Acknowledgment.* This work was supported by the Army Research Office MURI Grant W911NF-11-1-0362, the FAME Center, one of six centers of STARnet, a Semiconductor Research Corporation program sponsored by MARCO, DARPA, the U.S. Office of Naval Research MURI Grant N000014-09-1-1066 and MOE Academic Research Fund (AcRF) Tier 1 RG81/12 project Singapore and Si-COE project, Singapore. This work is also supported by the Singapore National Research Foundation under NRF RF Award No. NRF-RF2013-08, the start-up funding from Nanyang Technological University (M4081137.070).

*Supporting Information Available:* Additional HAADF-STEM images of $MoSe_2$ lattice and layer stacking; EELS spectra of $MoSe_2$. This material is available free of charge *via* the Internet at http://pubs.acs.org.

## REFERENCES AND NOTES


1. Kuc, A.; Zibouche, N.; Heine, T. Influence of Quantum Confinement on the Electronic Structure of the Transition Metal Sulfide $TS_2$. *Phys. Rev. B* **2011**, *83*, No. 245213.
2. Wang, Q. H.; Kalantar-Zadeh, K.; Kis, A.; Coleman, J. N.; Strano, M. S. Electronics and Optoelectronics of Two-Dimensional Transition Metal Dichalcogenides. *Nat. Nanotechnol.* **2012**, *7*, 699–712.
3. Chhowalla, M.; Shin, H. S.; Eda, G.; Li, L-J.; Loh, K. P.; Zhang, H. The Chemistry of Two-Dimensional Layered Transition Metal Dichalcogenide Nanosheets. *Nat. Chem.* **2013**, *5*, 263–275.
4. Mak, K. F.; Lee, C.; Hone, J.; Shan, J.; Heinz, T. F. Atomically Thin $MoS_2$: A New Direct-Gap Semiconductor. *Phys. Rev. Lett.* **2010**, *105*, 136805.
5. Splendiani, A.; Sun, L.; Zhang, Y.; Li, T.; Kim, J.; Chim, C-Y.; Galli, G.; Wang, F. Emerging Photoluminescence in Monolayer $MoS_2$. *Nano Lett.* **2010**, *10*, 1271–1275.
6. Wu, Z. Z.; Fang, B. Z.; Bonakdarpour, A.; Sun, A. K.; Wilkinson, D. P.; Wang, D. Z. $WS_2$ Nanosheets as a Highly Efficient Electrocatalyst for Hydrogen Evolution Reaction. *Appl. Catal., B* **2012**, *125*, 59–66.
7. Radisavljevic, B.; Radenovic, A.; Brivio, J.; Giacometti, V.; Kis, A. Single-layer $MoS_2$ Transistors. *Nat. Nanotechnol.* **2011**, *6*, 147–150.
8. Liu, H.; Neal, A. T.; Ye, P. D. Channel Length Scaling of $MoS_2$ MOSFETs. *ACS Nano* **2012**, *6*, 8563–8569.
9. Yin, Z.; Li, H; Li, H; Jiang, L; Shi, Y; Sun, Y; Lu, G; Zhang, Q; Chen, X; Zhang, H. Single-Layer $MoS_2$ Phototransistors. *ACS Nano* **2012**, *6*, 8563–8569.
10. Zeng, H. L.; Dai, J. F.; Yao, W.; Xiao, D.; Cui, X. D. Valley Polarization in $MoS_2$ Monolayers by Optical Pumping. *Nat. Nanotechnol.* **2012**, *7*, 490–493.
11. Cao, L. J.; Yang, S. B.; Gao, W.; Liu, Z.; Gong, Y. J.; Ma, L. L.; Shi, G.; Lei, S. D.; Zhang, Y. H.; Zhang, S. T.; *et al.* Direct Laser-Patterned Micro-Supercapacitors from Paintable $MoS_2$ Films. *Small* **2013**, *9*, 2905–2910.
12. Eda, G.; Maier, S. A. Two-Dimensional Crystals: Managing Light for Optoelectronics. *ACS Nano* **2013**, *7*, 5660–5665.
13. Yoon, J.; Park, W.; Bae, G-Y.; Kim, Y. H.; Jang, H. S.; Hyun, Y.; Lim, S. K.; Kahng, y. H.; Hong, W-K.; Lee, B. H.; *et al.* Highly Flexible and Transparent Multilayer $MoS_2$ Transistors with Graphene Electrodes. *Small* **2013**, *9*, 3295–3300.
14. Ross, J. S.; Wu, S.; Yu, H.; Ghimire, N. J.; Jones, A. M.; Aivazian, G.; Yan, J.; Mandrus, D. G.; Xiao, D.; Yao, W. Electrical Control of Neutral and Charged Excitons in a Monolayer Semiconductor. *Nat. Commun.* **2013**, *4*, No. 1474.
15. Tongay, S.; Zhou, J.; Ataca, C.; Lo, K.; Matthews, T. S.; Li, J. B.; Grossman, J. C.; Wu, J. Q. Thermally Driven Crossover from Indirect toward Direct Bandgap in 2D Semiconductors: $MoSe_2$ *versus* $MoS_2$. *Nano Lett.* **2012**, *12*, 5576–5580.
16. Najmaei, S.; Liu, Z.; Zhou, W.; Zou, X.; Shi, G.; Lei, S.; Yakobson, B. I.; Idrobo, J.-C.; Ajayan, P. M.; Lou, J. Vapour Phase Growth and Grain Boundary Structure of Molybdenum Disulphide Atomic Layers. *Nat. Mater.* **2013**, *12*, 754–759.
17. van der Zande, A. M.; Huang, P. Y.; Chenet, D. A.; Berkelbach, T. C.; You, Y.; Lee, G. H.; Heinz, T. F.; Reichman, D. R.; Muller, D. A.; Hone, J. C. Grains and Grain Boundaries in Highly Crystalline Monolayer Molybdenum Disulphide. *Nat. Mater.* **2013**, *12*, 554–561.
18. Ruizhitzky, E.; Jimenez, R.; Casal, B.; Manriquez, V.; Ana, A. S.; Gonzalez, G. PEO Intercalation in Layered Chalcogenides. *Adv. Mater.* **1993**, *5*, 738–741.
19. Bergmann, E.; Melet, G.; Muller, C.; Simonvermot, A. Friction Properties of Sputtered Dichalcogenide Layers. *Tribol. Int.* **1981**, *14*, 329–332.
20. Fan, F.-R. F.; White, H. S.; Wheeler, B.; Bard, A. J. Semiconductor Electrodes 0.29. High-Efficiency Photoelectrochemical Solar-Cells with N-$WSe_2$ Electrodes in an Aqueous Iodide Medium. *J. Electrochem. Soc.* **1980**, *127*, 518–520.
21. Chaparro, A. M.; Salvador, P.; Mir, A. The Scanning Microscope for Semiconductor Characterization (SMSC): Study of the Influence of Surface Morphology on the Photoelectrochemical Behavior of an N-$MoSe_2$ Single Crystal Electrode by Photocurrent and Electrolyte Electroreflectance Imaging. *J. Electroanal. Chem.* **1996**, *418*, 175–183.
22. Zhao, W. J.; Ghorannevis, Z.; Chu, L. Q.; Toh, M. L.; Kloc, C.; Tan, P. H.; Eda, G. Evolution of Electronic Structure in Atomically Thin Sheets of $WS_2$ and $WSe_2$. *ACS Nano* **2013**, *7*, 791–797.
23. Larentis, S.; Fallahazad, B.; Tutuc, E. Field-Effect Transistors and Intrinsic Mobility in Ultra-Thin $MoSe_2$ Layers. *Appl. Phys. Lett.* **2012**, *101*, 223104.
24. Kristl, M.; Drofenik, M. Synthesis of Nanocrystalline $MoSe_2$ by Sonochemical Reaction of Se with $Mo(CO)_6$. *Inorg. Chem. Commun.* **2003**, *6*, 68–70.
25. Zhan, J. H.; Zhang, Z. D.; Qian, X. F.; Wang, C.; Xie, Y.; Qian, Y. T. Synthesis of $MoSe_2$ Nanocrystallites by a Solvothermal Conversion from $MoO_3$. *Mater. Res. Bull.* **1999**, *34*, 497–501.
26. Li, H.; Lu, G.; Wang, Y. L.; Yin, Z. Y.; Cong, C. X.; He, Q. Y.; Wang, L.; Ding, F.; Yu, T.; Zhang, H. Mechanical Exfoliation and Characterization of Single- and Few-Layer Nanosheets of $WSe_2$, $TaS_2$, and $TaSe_2$. *Small* **2012**, *9*, 1974–1981.
27. Coleman, J. N.; Lotya, M.; O'Neill, A.; Bergin, S. D.; King, P. J.; Khan, U.; Young, K.; Gaucher, A.; De, S.; Smith, R. J. Two-Dimensional Nanosheets Produced by Liquid Exfoliation of Layered Materials. *Science* **2011**, *331*, 568–571.
28. Bougouma, M.; Batan, A.; Guel, B.; Segato, T.; Legma, J. B.; Reniers, F.; Delplancke-Ogletree, M.-P.; Buess-Herman, C.; Doneux, T. Growth and Characterization of Large, High Quality $MoSe_2$ Single Crystals. *J. Cryst. Growth* **2013**, *363*, 122–127.
29. Yu, Q. K.; Jauregui, L. A.; Wu, W.; Colby, R.; Tian, J. F.; Su, Z. H.; Cao, H. L.; Liu, Z. H.; Pandey, D.; Wei, D. G.; *et al.* Control and Characterization of Individual Grains and Grain Boundaries in Graphene Grown by Chemical Vapour Deposition. *Nat. Mater.* **2011**, *10*, 443–449.
30. Sun, Z. Z.; Yan, Z.; Yao, J.; Beitler, E.; Zhu, Y.; Tour, J. M. Growth of Graphene from Solid Carbon Sources. *Nature* **2010**, *468*, 549–552.
31. Bae, S.; Kim, H.; Lee, Y.; Xu, X.; Park, J.-S.; Zheng, Y.; Balakrishnan, J.; Lei, T.; Kim, H. R.; Song, Y., Il.; *et al.* Roll-to-roll Production of 30-in. GrapheneFilms for Transparent Electrodes. *Nat. Nanotechnol.* **2010**, *5*, 574–578.
32. Song, L.; Ci, L.; Lu, H.; Sorokin, P. B.; Jin, C.; Ni, J.; Kvashnin, A. G.; Kvashnin, D. G.; Lou, J.; Yakobson, B. I.; *et al.* Large Scale Growth and Characterization of Atomic Hexagonal Boron Nitride Layers. *Nano Lett.* **2010**, *10*, 3209–3215.
33. Kim, K. K.; Hsu, A.; Jia, X.; Kim, S. M.; Shi, Y.; Hofmann, M.; Nezich, D.; Rodriguez-Nieva, J. F.; Dresselhaus, M.; Palacios, T.; *et al.* Synthesis of Monolayer Hexagonal Boron Nitride on Cu Foil Using Chemical Vapor Deposition. *Nano lett.* **2011**, *12*, 161–166.
34. Lee, Y. H.; Zhang, X.-Q.; Zhang, W.; Chang, M.-T.; Lin, C.-T.; Chang, K.-D.; Yu, Y.-C.; Wang, J. T.-W.; Chang, C.-S.; Li, L.-J.; *et al.* Synthesis of Large-Area $MoS_2$ Atomic Layers with Chemical Vapor Deposition. *Adv. Mater.* **2012**, *24*, 2320–2325.
35. Peimyoo, N.; Shang, J.; Cong, C.; Shen, X.; Wu, X.; Yeow, K. L.; Yu, T. Non-Blinking Intense Two-Dimensional Light Emitter: Monolayer $WS_2$ Triangles. *ACS Nano* **2013**, *7*, 10985–10994.

36. Zhang, Y.; Zhang, Y.; Ji, Q.; Ju, J.; Yuan, H.; Shi, J.; Gao, T.; Ma, D.; Liu, M.; Chen, Y.; *et al.* Controlled Growth of High-Quality Monolayer $WS_2$ Layers on Sapphire and Imaging Its Grain Boundary. *ACS Nano* **2013**, *7*, 8963–8971.
37. Huang, J.-K.; Pu, J.; Hsu, C.-L.; Chiu, M.-H.; Juang, Z.-Y.; Chang, Y.-H.; Chang, W.-H.; Iwasa, Y.; Takenobu, T.; Li, L.-J. Large-Area Synthesis of Highly Crystalline $WSe_2$ Monolayers and Device Applications. *ACS Nano* **2013**, *8*, 923–930.
38. Li, H.; Zhang, Q.; Yap, C. C. R.; Tay, B. K.; Teo, H. T.; Olivier, A.; Baillargeat, D. From Bulk to Monolayer $MoS_2$: Evolution of Raman Scattering. *Adv. Funct. Mater.* **2012**, *22*, 1385–1390.
39. Eda, G.; Yamaguchi, H.; Voiry, D.; Fujita, T.; Chen, M.; Chhowalla, M. Photoluminescence from Chemically Exfoliated $MoS_2$. *Nano Lett.* **2011**, *11*, 5111–5116.
40. Horzum, S.; Sahin, H.; Cahangirov, S.; Cudazzo, P.; Rubio, A.; Serin, T.; Peeters, F. M. Phonon Softening and Direct to Indirect Band Gap Crossover in Strained Single-layer $MoSe_2$. *Phys.Rev. B* **2013**, *87*, 125415.
41. Tonndorf, P.; Schmidt, R.; Böttger, P.; Zhang, X.; Börner, J.; Liebig, A.; Albrecht, M.; Kloc, C.; Gordan, O.; Zahn, D. R. T.; *et al.* Photoluminescence Emission and Raman Response of monolayer $MoS_2$, $MoSe_2$, and $WSe_2$. *Opt. Express* **2013**, *21*, 4908–4916.
42. Gong, Y.; Liu, Z.; Lupini, A. R.; Shi, G.; Lin, J.; Najmaei, S.; You, G.; Terrones, H.; Terrones, M.; Vajtai, R.; *et al.* Band Gap Engineering and Layer-by-Layer Mapping of Selenium-Doped Molybdenum Disulfide. *Nano Lett.* **2014**, *14*, 442–449.
43. Zhan, Y.; Liu, Z.; Najmaei, S.; Ajayan, P. M.; Lou, J. Large-area Electrical Control of Neutral and Charged Excitons in a Monolayer Semiconductor Vapor-phase Growth and Characterization of $MoS_2$ Atomic Layers on a $SiO_2$ Substrate. *Small* **2012**, *8*, 966–971.